J Therm Anal Calorim (2012) 108:1223–1234
DOI 10.1007/s10973-011-1652-0

A comprehensive assessment on degradation of multi-walled carbon nanotube-reinforced EMA nanocomposites

U. Basuli · T. K. Chaki · D. K. Setua · S. Chattopadhyay

Received: 13 April 2011 / Accepted: 10 May 2011 / Published online: 26 May 2011

Abstract Thermal degradation kinetics of MWNT-reinforced EMA-based nanocomposites having different methyl acrylate (MA) contents (by % mass) ranging from 9 to 30% have been monitored. Kissinger and Flynn–Wall–Ozawa methods for evaluating non-isothermal degradation of polymers have been examined. Overall, the thermal stabilities of the nanocomposites are the function of amount of MWNTs loading and their state of dispersion that depends on the MA content of respective EMAs. Composite samples exhibit higher activation energy (E_a) than the neat EMAs but the E_as of the composites diminish with increased MA contents of the matrices. TG-Mass spectrometry has been used to identify the volatile products resulting from thermal degradation of composites, and a promising mechanism has been proposed over different range of temperatures of degradation. It is proposed that the side-group scission of methoxycarbonyl group initiates thermal decomposition following combination of chain end and random chain scission reactions, ensuing pseudo second-order kinetics.

Keywords Non-isothermal and isothermal kinetics · EMA · MWNT · Nanocomposites · Dispersion · TG-mass spectrometry

U. Basuli · T. K. Chaki · S. Chattopadhyay (✉)
Rubber Technology Centre,
Indian Institute of Technology,
Kharagpur 721302, India
e-mail: santanuchat71@yahoo.com

D. K. Setua
DMSRDE, Kanpur, India

Introduction

The study of degradation and stabilization of polymers is an extremely important area from the scientific, industrial, environment, and safety point of views. Thermo gravimetric analysis (TG) is an excellent tool for studying the kinetics of thermal degradation of polymeric samples. The thermal analysis is applied to any technique which involves a measurement of a material's specific property while the temperature is controlled and monitored [1, 2]. When a polymer sample degrades, its major mass loss is due to the production of gaseous products, like water vapor, hydrocarbons, carbon monoxide, and carbon dioxide. It is essential to understand the thermal degradation pathways of polymers and also to realize the influence of additives on the degradation, to control, to accelerate, or to retard the degradation pathways. Additional mechanistic information is usually obtained if the degradation is carried out at modest environment, controlled temperatures, and at different heating rates. TG is widely used because of its experimental simplicity and the wealth of information that can be derived from a simple TG curve [3]. Carbon fiber is commonly used reinforcing filler in many matrices, such as, polymers, metals, and ceramics materials. Compared to carbon fibers, carbon nanotubes (CNTs) have larger aspect ratio, higher modulus, and lower density in addition to their exceptional electrical and optical properties [4]. Thus, the properties of CNT composites have attracted much attention, both for scientific interest and practical applications [5–7]. Several ways to perform kinetic studies of the degradation of polymeric materials are already known. TG analyses combining various non-isothermal kinetic methods are widely used for this purpose [8–12].

Commercial ethylene methyl acrylate (EMA) copolymers are semi-crystalline polymer having the lowest

density among the major plastics, and they possess a very high strength to mass ratio. EMA exhibits excellent thermal stability and good mechanical properties, high chemical resistance, and low dielectric constant [13]. The knowledge of thermal stability and thermal degradation kinetics are significant for the production and application. The effects of MWNTs on the properties of EMA/MWNT system, selective dispersion, and distribution of MWNTs in EMA matrices have been reported in our previous study [14, 15]. The thermal degradation and dynamic mechanical behavior of LLDPE/EMA blends have been investigated by Borah and Chaki [16]. Thermal decomposition of MWNTs and modified MWNTs has been first characterized by Chou et al. [17].

From the literature review, it is realized that no fundamental kinetics analysis has been made to understand the degradation behavior of EMA system.

In this study, an attempt has been made to explore the thermal degradation behavior of MWNTs-filled EMA-based systems. Detailed non-isothermal and isothermal kinetic analyses of the nanocomposites and neat system have been performed to realize their degradation behavior at different heating rates under nitrogen atmosphere (using different kinetic methods). Since the process of chain scission is very complex, it leads to a mixture of fragments by either random or specific manner, depending on the experimental conditions. The gaseous products resulted during the thermal degradation have been evidenced, and analysis of gaseous products by TG with mass detector has also been performed. An attempt has been made to understand the influence of MA content on the overall fragmentation process of these composites.

Experimental

Materials

Three commercial grades of EMA (duPont, USA), Elvaloy® 1209 (EMA09), Elvaloy® 1224 (EMA24), and Elvaloy® 1330 (EMA30), respectively, were chosen as the matrices of MWNT-based nanocomposites. The general characteristics of Elvaloy® grades of EMA used in this study are given in Table 1 below. This is important since the degradation pathways could be related with these factors.

MWNTs were purchased from Helix Material Solutions, USA and used as received. MWNTs were prepared by the chemical vapor deposition (CVD) process having purity of about 95%, average diameter of about 40–60 nm, and average length of about 0.5–40 μm (data provided by the manufacturer). Toluene used as a solvent for EMA was obtained from Merck Specialties Private Limited, Mumbai, India.

Preparation of polymer/MWNTs composite

Dispersion of MWNTs in toluene were prepared by exposing them to ultra-sonic vibration for total of 30 min keeping intervals of 5 min after each 5 min of sonication to minimize the heat build up during this process. 5% solution of EMA in toluene was prepared, which was combined with the pre-dispersed MWNTs in toluene. The mixture was sonicated for another 30 min to achieve homogeneous dispersion/distribution. It was then cast on flat glass surfaces, and solvent was allowed to evaporate slowly at room temperature. Subsequently, the films were dried under vacuum at 50 °C for 3 h, and the resulting films had an average thickness of 0.85 mm. A series of EMA/MWNT composite films were prepared with different mass concentrations of MWNTs. To achieve a better length scale of dispersion and distribution of MWNTs, the films obtained by solution mixing and casting (described earlier) were further melt-mixed separately using a HAAKE Rheomix OS (Germany) at 120 °C for 5 min. The rotor speed was maintained at 50 rpm with a fill factor of 75%. Immediately after mixing, the molten mass was passed through the nip of a two-roll mill kept at ambient temperature to obtain a sheet of about 3-mm thickness. The sheets were molded at 120 °C for 4 min in a compression-molding machine (Moore Press, United Kingdom) equipped with water cooling system. Teflon sheets were placed between the molded sheet and the press plates. The sheet was then cooled at room temperature under pressure. The average thicknesses of the resulting sheets were approximately 2 mm. Sample designations are given according to the following: E = EMA, N = MWNTs, the number after E = % of MA content in EMA, and the number after

Table 1 Properties of EMA (Co-polymer of ethylene and MA)

Grades of EMA	Melt flow index/MFI[a]	Density/g cm^{-3}	DSC melting point/°C	Crystallinity/%	% of MA
Elvaloy® 1209	2.0	0.927	101	30.3	9
Elvaloy® 1224	2.0	0.944	91	13.8	24
Elvaloy® 1330	3.0	0.950	85	7.2	25

[a] ASTM D1238 and ISO 1133 in g/10 min

N = % of MWNTs. Thus, E09N1.0 denotes a sample of EMA/MWNT composite containing EMA with 9% MA loaded with 1.0% MWNTs.

Morphological characteristics

High-resolution transmission electron microscopy (HRTEM) was carried out on JEM 2100, JEOL make, Japan, transmission electron microscope equipped with lanthanum hexa-boride target, operating at 200 kV and with beams current of 116 μA. Samples were cut to 50-nm thickness using Leica Ultracut EM FCS, ultracryotom, Austria. The cut samples were supported on a copper mesh before observation under the microscope.

Non-isothermal TG measurements

TG measurements were performed with 10–12 mg of samples using a TGA Q50 V6.1, TA Instruments, USA, under a nitrogen atmosphere from room temperature (~30 °C) to 600 °C operated in the dynamic mode at different heating rates of 5, 10, 15, and 20 °C min^{-1}, respectively. Samples were placed into a platinum pan, and the experiments were conducted in nitrogen atmosphere. For each sample, three tests were carried out under the same heating rate, and the characteristic temperatures were reproducible to ±1.0 °C. The analyses of the TG data were done using TA Instrument's Universal Analysis software. The same software was used for kinetic analysis of non-isothermal data recorded at four heating rates. In this experiment, the temperature corresponding to 5% degradation was taken as the degradation onset temperature (T_{onset}). In addition, the temperature corresponding to the maximum value (T_{max}) in the derivative TG curve was also recorded. Percentage error in such thermal measurements was limited to ±2%. The values of $T_{onset,}$ T_{max}, and mean activation energy (E_a) reported in the Table 3 are the average of three values. The conversion values 5, 8, 11, 14, 17, and 20% have been used to derive the E_a using the Flynn–Wall–Ozawa method.

Limited information can be obtained especially about the chemistry of the decomposition by TG experiment alone. TG in conjunction with mass spectrometry (TG/MS) can provide insights regarding actual degradation path and kinetics from the overall mass loss and yields of the final gaseous products. The products of thermal degradation were analyzed by the method of mass-spectrometric thermal analysis. The samples, located in the Ar atmosphere, were heated from room temperature to 600 °C at a rate of 10 °C min^{-1}, and at the same time the different gaseous products of their thermal degradation were detected with a GD 300T mass spectrometer, Balzers Instruments, Germany. The mass range scanned was restricted up to 300 amu.

Isothermal TG measurements

The isothermal tests were carried out in nitrogen atmosphere at 375, 400, 425, and 450 °C, respectively for 60 min using the same TG instrument as depicted earlier. Before isothermal heating, the sample was heated at a rate of 30 °C min^{-1} from ambient temperature to the selected temperature of isothermal degradation. As soon as the system reached the selected temperature, the variations of sample mass with times were registered.

Analytical techniques

Kinetic methods [18]

The reaction rate in TG studies can be defined as the variation of degree of conversion (α) with time or temperature, and the conversion is typically calculated as:

$$\alpha = \frac{W_0 - W_t}{W_0 - W_f} \tag{1}$$

where W_0, W_t, and W_f are, respectively, mass at the beginning of the degradation step, actual mass at each point of the curve, and the final mass measured after the specific degradation process considered. All kinetic studies assume that the isothermal rate of conversion, $d\alpha/dt$, is a linear function of a temperature-dependent rate constant, $k(T)$, and a temperature-independent function of the conversion, α, i.e.,

$$\frac{d\alpha}{dt} = k(T)f(\alpha) \tag{2}$$

where $f(\alpha)$ depends on the mechanism of the degradation reaction. The function $k(T)$ is usually described by the Arrhenius equation as:

$$k(T) = Ae^{-\frac{E_a}{RT}} \tag{3}$$

where A, E_a, R, and T are the pre-exponential factor (min^{-1}) assumed to be independent of temperature, the activation energy (kJ mol^{-1}), the universal gas constant (8.314 J mol^{-1} K^{-1}), and the absolute temperature (K), respectively.

Combination of Eqs. 2 and 3 yields the following expression:

$$\frac{d\alpha}{dt} = Af(\alpha)e^{-\frac{E_a}{RT}} \tag{4}$$

At constant heating rate, $\beta = dT/dt$, and Eq. 4 may be written as the following:

$$\beta \frac{d\alpha}{dT} = Af(\alpha)e^{-\frac{E_a}{RT}} \quad (5)$$

Integration of Eq. 5 within the limits of an initial temperature, T_0, corresponding to a degree of conversion α_0 and the peak temperature, T_p, corresponding to a degree of conversion α_p, gives the following expression:

$$\int_{\alpha_0}^{\alpha_p} \frac{d\alpha}{f(\alpha)} = \frac{A}{\beta} \int_{T_0}^{T_P} e^{-\frac{E_a}{RT}} dT \quad (6)$$

The integral function of conversion, $g(\alpha)$, is obtained if T_0 is low and hence assuming that $\alpha = 0$ and also considering that there is no reaction within a temperature range of 0 and T_0 as:

$$g(\alpha) = \int_{0}^{\alpha_p} \frac{d\alpha}{f(\alpha)} = \frac{A}{\beta} \int_{0}^{T_P} e^{-\frac{E_a}{RT}} dT \quad (7)$$

Kissinger's method [11]

Kissinger's method is one of the differential methods which have been used by researchers to determine the E_a of solid-state reactions from plots of the logarithm of the heating rate versus the inverse of the temperature. T_{max} is used at different heating rate to compute the activation energy. The beauty of this method is that even without a precise knowledge of the reaction mechanism [19, 20], the E_a can be determined using the following equation:

$$\ln \frac{\beta}{T^2} = \ln \frac{AR}{Eg(\alpha)} - \frac{E_a}{RT} \quad (8)$$

where β is the heating rate, T is the temperature corresponding to the inflection point of the thermal degradation curves which correspond to the maximum rate, A is the pre-exponential factor, E_a is the activation energy, α_{max} is the maximum conversion, and n is the order of the reaction. From a plot of ln (β/T^2_{max}) versus $1000/T_{max}$ and fitting to a straight line, E_a can be calculated from the slope.

Flynn–Wall–Ozawa method

This iso-conversional integral method suggested independently by Ozawa [21] and Flynn and Wall [22] uses Doyle's approximation [23] of the temperature integral. From Eq. 7 and using Doyle's approximation, the logarithm of the integrated results leads to the Flynn–Wall–Ozawa equation:

$$\log \beta = \log \frac{AE_a}{Rg(\alpha)} - 2.315 - \frac{0.457E_a}{RT} \quad (9)$$

where α, β, A, E_a, R, and T have their usual significance. Thus, for α = constant, the plot of log β versus $1000/T$ obtained at several heating rates should yield a straight line whose slope can be used to evaluate the E_a.

Using this integral method, one can determine the E_a without the knowledge of reaction order at different levels of conversion. Owing to the fact that Eq. 9 was derived considering the Doyle approximation, the equation can be effectively used within a limited conversion values.

Results and discussion

Morphological characteristics

Figure 1a–c shows representative the HRTEM photomicrographs of the EMA09, EMA24, and EMA30-based composites with 2.5% MWNTs loading. The figures show that the nanotubes are randomly oriented in the polymer matrix. From Fig. 1a, it can be found that distribution of MWNTs are more homogeneous and less entangled in the EMA09 matrix. This phenomenon occurs by the increased interfacial bonding between the MWNTs and the EMA09 matrixes. Figure 1b shows inferior dispersion, with a few areas showing sign of aggregation of nanotubes; while in EMA30 matrix (highest MA content), MWNTs are acutely entangled, forming agglomeration or clusters inside the matrix. MWNTs dispersed in the polymer matrix exist in the form of agglomerates and aggregated as shown in Fig. 1c. In E09N2.5 composite, MWNTs are more uniformly dispersed. Overall, dispersion of MWNTs is significantly poor in EMA30. Limited degrees of breakdown of MWNTs are also noticed especially for E09N2.5.

Effect of pristine MWNTs on thermal degradation of EMA/MWNT composites

The TG experiments of different nanocomposites have been carried out at different heating rates (5, 10, 15, and 20 °C min^{-1}) under Nitrogen atmosphere in the temperature range of 35–600 °C. Figure 2a, b depicts the representative TG curves of the pristine EMA09, EMA24, and EMA30 and their composites with 1.0, 2.5% MWNTs loading at a heating rate of 10 °C min^{-1}. The major decomposition region is centered between 350 and 500 °C. For the composites with EMA24 and EMA30, the thermal stabilities are not too different from their respective matrices. Relative to pure EMA09, in its composites, the degradation becomes slower. The all TG curves of EMA and their nanocomposites show apparently single-step degradation, but when the decomposition pattern is observed minutely, it reveals a two-stage degradation behavior (when the curves are fitted using multi-Gaussian deconvolution results in two overlapping Gaussian curves) [15]. This divulges the well-defined initial and final

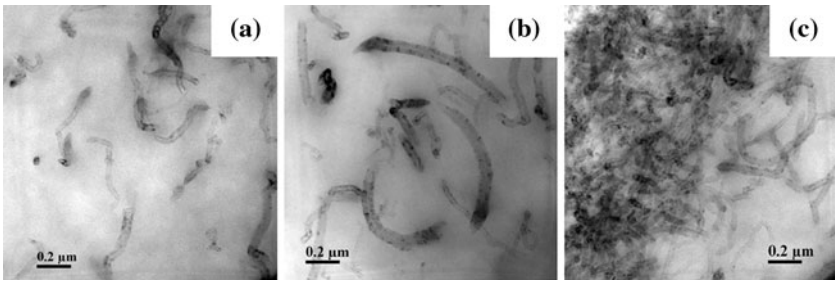

Fig. 1 HRTEM photomicrograph (at ×12 k magnification) of MWNT/EMA composites: **a** E09N2.5, **b** E24N2.5, and **c** E30N2.5

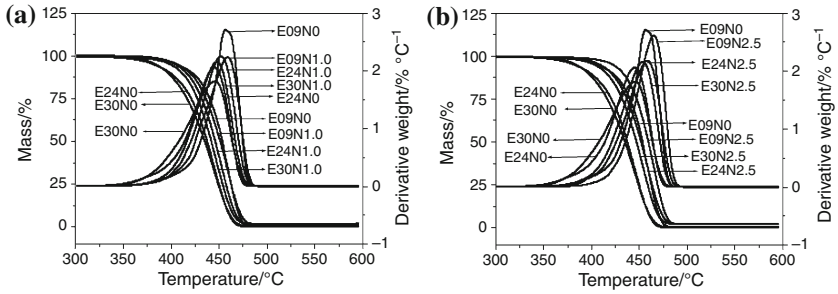

Fig. 2 **a**, **b** TG curves of pure EMA and its various nanocomposites

Table 2 Parameters obtained from TG analysis

Sample no.	*T* 5% loss/°C	*T* 10% loss/°C	*T* 20% loss/°C	*T* 30% loss/°C	*T* 50% loss/°C	*T* 70% loss/°C	*T* 80% loss/°C	T_{max}/°C
E09N0	405.5	420.0	435.8	443.6	453.4	460.8	464.4	456.6
E09N1.0	407.5	419.6	431.8	439.6	451.2	460.4	464.9	459.0
E09N2.5	422.7	433.1	443.6	450.1	459.4	467.3	471.1	465.5
E24N0	383.7	398.8	415.6	425.0	437.5	447.4	452.3	445.5
E24N1.0	404.2	416.0	427.8	435.2	446.0	454.6	459.6	452.0
E24N2.5	409.0	420.8	432.9	440.7	451.7	461.0	465.9	458.5
E30N0	381.8	396.7	411.2	421.1	435.1	446.3	451.9	445.0
E30N1.0	399.4	411.2	423.3	430.7	441.8	451.0	456.1	447.5
E30N2.5	403.4	415.7	427.8	435.9	447.0	456.4	461.2	453.6

degradation temperatures. Initial step in the degradation of EMA involves the decomposition of carbonyl side groups. The second step is possibly associated with the degradation of the main chains [14, 15]. The degradation curve for the pure EMA24 runs in between to those of the pristine EMA09 and pristine EMA30. In fact, in case of all pure EMAs, no significant residue was left after the end of TG experiment. The characteristic parameters obtained from TG are summarized in Table 2. From Table 2, no drastic improvement in the thermal stability is observed for the filled systems compared to the pristine polymers especially for EMA24 and EMA30. A modest degree of improvement is observed only in case of E09N2.5. In our previous study, we have reported that the thermal stability of EMA30 was not improved significantly after addition of MWNTs; while EMA09 can be stabilized fairly with MWNTs [15].

Kinetics of thermal decomposition

Typical Kissinger plots for various composites are shown in Fig. 3a–c. The E_a has been estimated from the slope of a straight line obtained from the plot of ln (β/T_{max}^2) versus $1000/T_{max}$ (plots are not shown). A very good correlation coefficient of fitment (R^2 value > 0.95) has been obtained. The slope obtained from above plot is used to calculate the E_a. All figures show that the linearly fitted straight lines are nearly parallel and thus confirm the applicability of these methods within the conversion range studied. Similar plots have also been obtained with more than 93–95% confidence for the other nanocomposites (not shown here). The characteristic temperatures and the mean E_a for thermal degradation of EMAs and their respective nanocomposites as calculated by the Kissinger technique are summarized in Table 3. The E_a of the pristine EMAs are lower than those of the filled composites in general. However, E_as of EMA30-based composites are surprisingly lower than those of the other composites. A similar trend has been observed with the 1.0% loaded composites. This implies that the thermal stability of E09N2.5 is more than both of the E24N2.5 and E30N2.5. The E_a values increase with increasing MWNT content up to 2.5% for EMA09-based composites because of the increasing thermal stability and

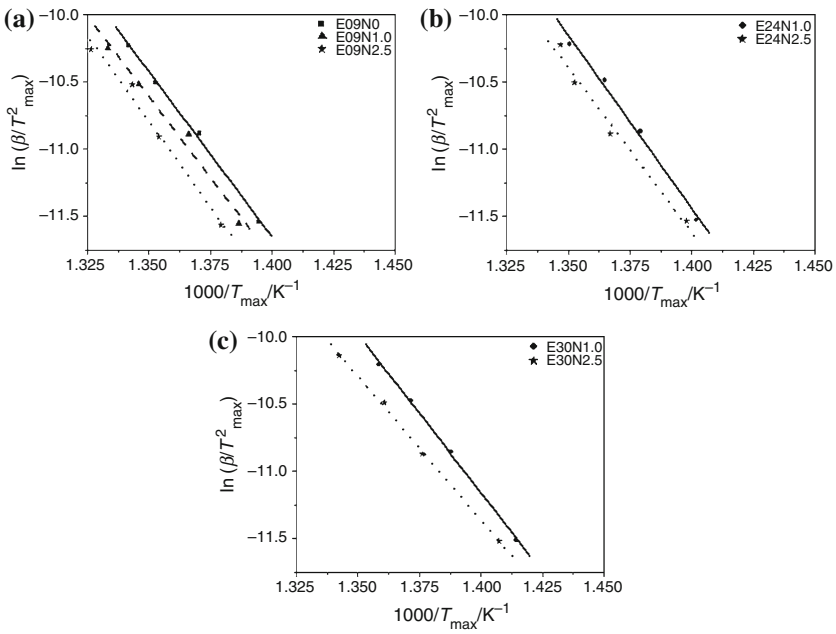

Fig. 3 **a–c** Typical Kissinger plot from the experimental data at different heating rates

Table 3 Kinetic parameters for the thermal degradation of various EMA/MWNTs composites

Sample code	Parameter	Heating rate/°C min^{-1}				Mean activation energy, E_a/kJ mol^{-1}	
		5	10	15	20	Kissinger	Flynn–Wall–Ozawa
E09N0	T_{onset}	390.0	405.5	417.1	419.2	200	167
	T_{max}	445.1	456.6	466.2	471.9		
E09N1.0	T_{onset}	401.0	407.5	423.7	431.9	213	175
	T_{max}	450.2	459.0	470	477.0		
E09N2.5	T_{onset}	408.0	422.7	429.4	431.2	236	203
	T_{max}	455.0	465.5	471.5	480.9		
E24N0	T_{onset}	383.0	383.7	408.7	415.5	190	162
	T_{max}	436.7	445.5	458.4	464.4		
E24N1.0	T_{onset}	391.5	404.2	411.2	419.0	211	186
	T_{max}	440.3	452.0	459.7	467.5		
E24N2.5	T_{onset}	394.5	409.0	418.2	420.3	205	185
	T_{max}	442.3	458.5	466.4	469.5		
E30N0	T_{onset}	380.5	381.8	388.0	410.4	183	117
	T_{max}	439.0	445.0	448.0	464.0		
E30N1.0	T_{onset}	385.0	399.4	408.8	413.8	195	169
	T_{max}	434.0	447.5	456.0	463.0		
E30N2.5	T_{onset}	391.5	403.4	415.1	419.0	180	174
	T_{max}	437.5	453.6	461.9	453.6		

T_{onset} was determined from the respective TG curve with 5 wt% loss

T_{max} was determined from the respective DTG curve peaks

state of dispersion of MWNT in the composites. The secondary forces involved between the polymer chains and surface of the nanotube lead to trapped entanglements, which play a role of physical cross linking, thus causing greatly enhanced E_a of the matrix. Whereas, for EMA24-based composites, the E_a values increase with increasing MWNT content up to 1%, then it decreases at 2.5% MWNTs loading. Enhanced polarity of EMA due to increased MA content may reduce polymer–nanotube interactions. In addition, it can be noted that the E_a corresponding to different percentages of MWNTs decreases with the increase in MA content irrespective of amount of

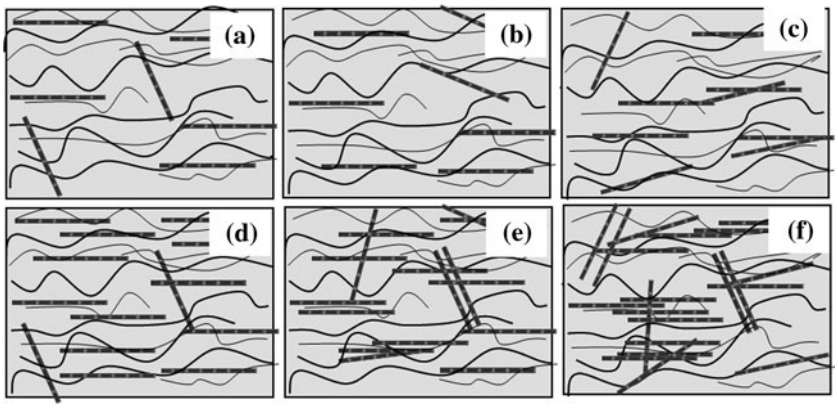

Scheme 1 Schematic depiction of inherent morphology of composites: **a** E09N1.0, **b** E24N1.0, **c** E30N1.0, **d** E09N2.5, **e** E24N2.5, and **f** E30N2.5

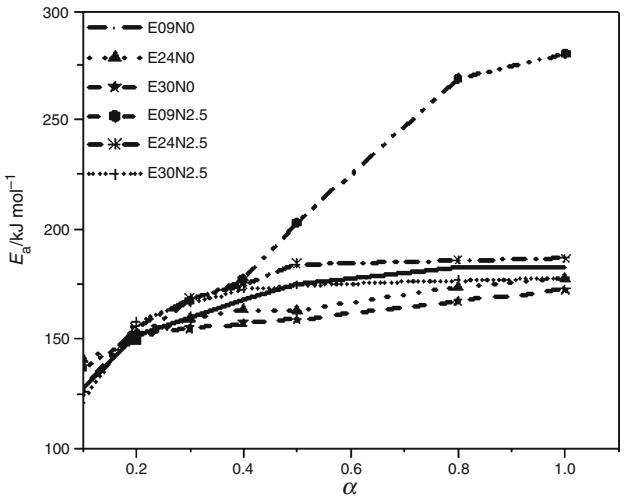

Fig. 4 Activation energies values with conversion degree for pristine EMA and their respective composites

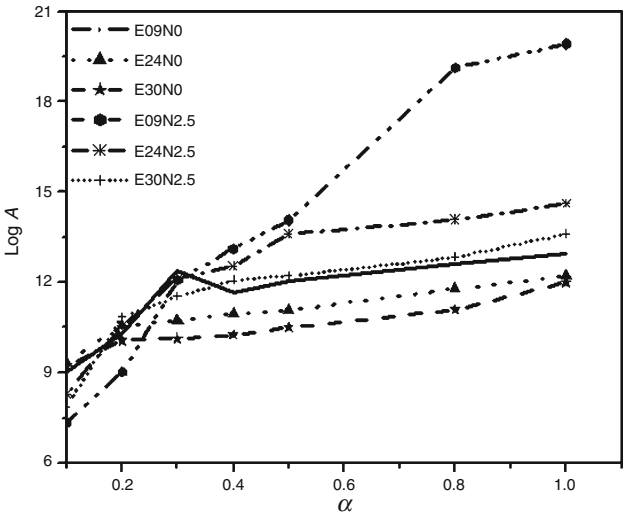

Fig. 5 Variation of pre-exponential factor (A) values with conversion degree for pristine EMA and their respective composites

MWNTs present inside the matrix polymers. A scheme has been proposed (Scheme 1a–f) to elucidate the possible morphology of the composites based on our earlier studies [15] to explain the above observations. These reflect large scale aggregation of MWNTs in E30N2.5 composite, but in E24N2.5 composites, the extent of aggregations are substantially less. The barrier effects originating from the dispersion of the nanotubes in the polymer may possibly hinder diffusion of decomposition products into the bulk of the material. This has also been evident when the pristine EMAs leave no residue at a temperature higher than 500 °C whereas, the residues are significant in the presence of the MWNTs in the EMA matrices.

The kinetic parameters, such as, the E_a and pre-exponential factor (A) which characterize the thermal decomposition process were calculated. The results obtained using Flynn–Wall–Ozawa methods are presented in Figs. 4 and 5. The lower degree of conversion (α) range of 0.1–1.0 was taken into account. The increased in E_a and log A with the increase of α is indicative of complex reactions during decomposition (involving several mechanisms) [24]. This variation of E_a, especially at higher α, is a sign of the process complexity. For pure EMA30, in particular, the trend of variation of kinetic parameters with conversion can possibly be explained on the basis of enhanced complication of thermal degradation mechanism at higher temperatures.

However, from application point of view, for polymeric materials, onset of degradation is the most important factor. The mean E_a obtained using the Flynn–Wall–Ozawa method is also listed in Table 3, and typical Flynn–Wall–Ozawa plots for E09N2.5, E24N2.5, and E30N2.5 are shown in Fig. 6a, b, and c, respectively. Figures show that the best fit straight lines are nearly parallel and thus confirm the applicability of this method within the conversion range studied. The E_a values computed using Flynn–Wall–Ozawa method also show that the thermal stability of the samples decreases in the following way: E09N2.5 > E24N2.5 > E30N2.5.

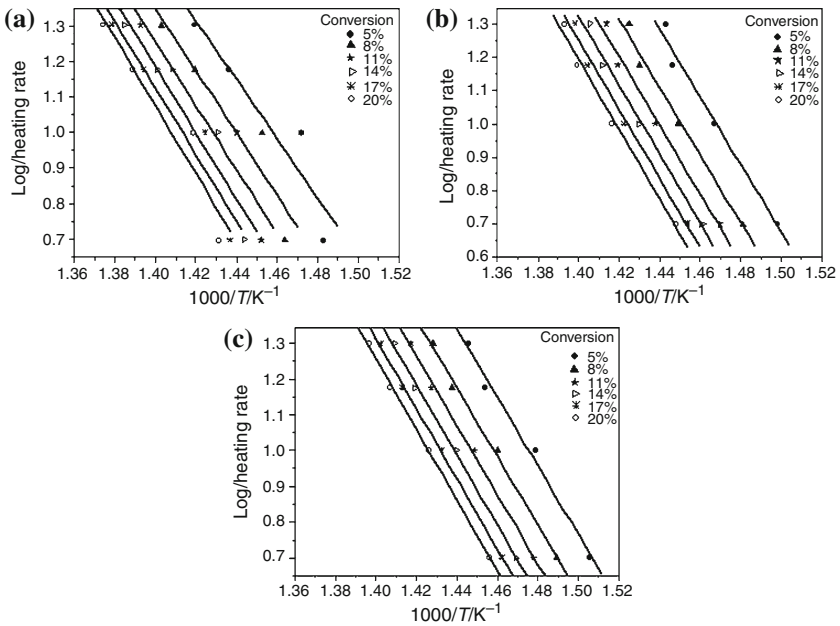

Fig. 6 Typical Flynn–Wall–Ozawa plots for **a** E09N2.5, **b** E24N2.5, and **c** E30N2.5

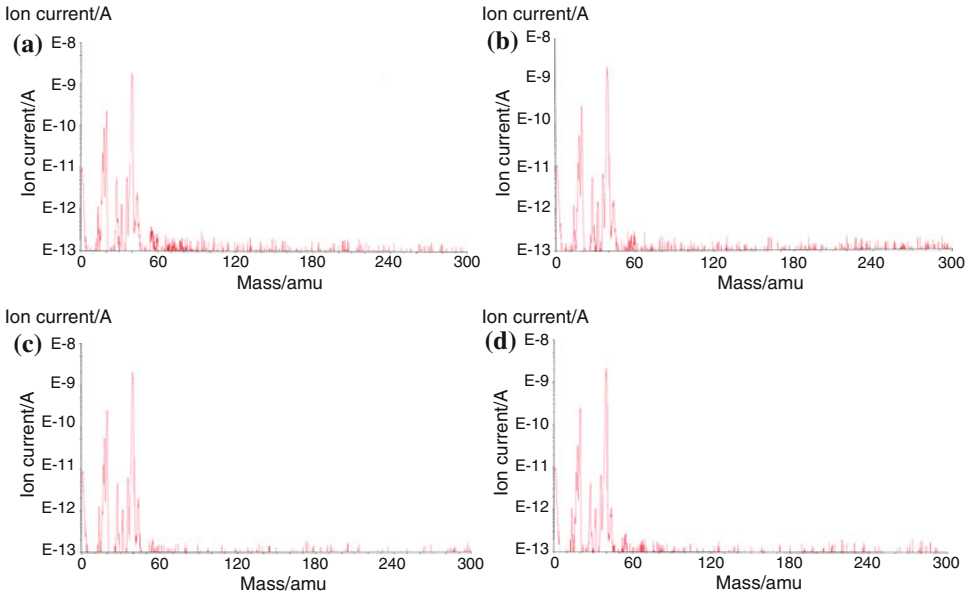

Fig. 7 TG-mass spectroscopy: **a** E09N0 about at 270 °C, **b** E09N2.5 about at 270 °C, **c** E09N0 about at 450 °C, and **d** E09N2.5 about at 450 °C

A similar trend in the thermal stability of the samples is reflected from both Kissinger and Flynn–Wall–Ozawa methods, corresponding to E_a of the samples. However, both methods have some difficulties in calculating kinetic parameters such as reaction order, pre-exponential factor, etc.

TG-mass spectroscopy

Decomposition products of polymers have been determined by many investigators, but the results are often conflicting because of difficulties in analyzing a large number of products. A comprehensive analysis of the thermal decomposition products of EMA has been made with the help of TG-mass spectroscopy techniques. It is obvious from Figs. 7, 8, and 9 that a very large number of products are produced under these conditions. The structures for most of the compounds as obtained from above scans were determined. The evidence supporting the proposed mechanism is based on smaller fragments. The initiation of thermal degradation involves the loss of a hydrogen atom from the polymer chain as a result of energy input from heat. This creates a highly reactive and unstable polymer 'free radical' and a hydrogen atom with an unpaired electron. Groups that are attached to the side of the backbone are held by bonds which are weaker than the bonds

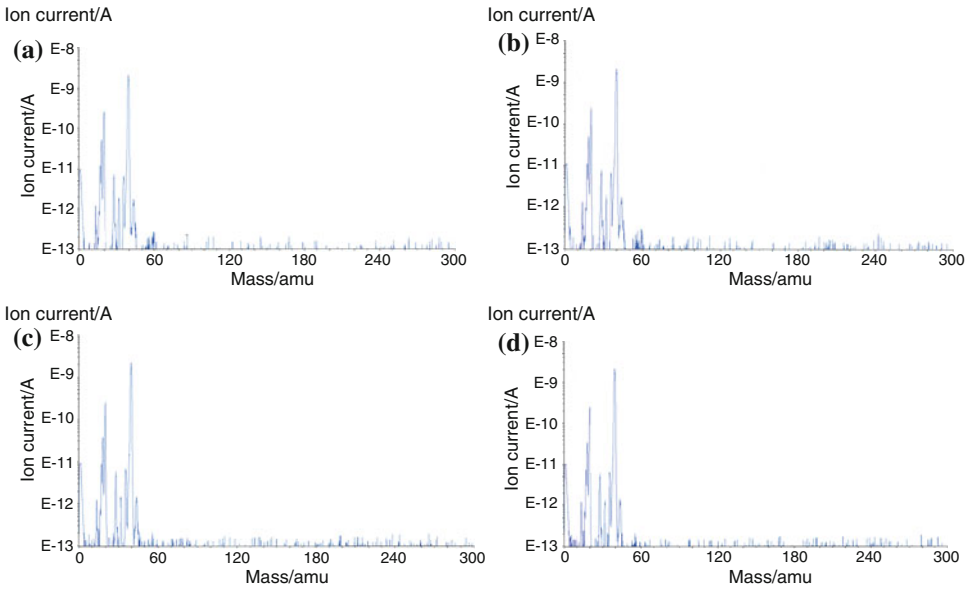

Fig. 8 TG-mass spectroscopy: **a** E24N0 about at 270 °C, **b** E24N2.5 about at 270 °C, **c** E24N0 about at 450 °C, and **d** E24N2.5 about at 450 °C

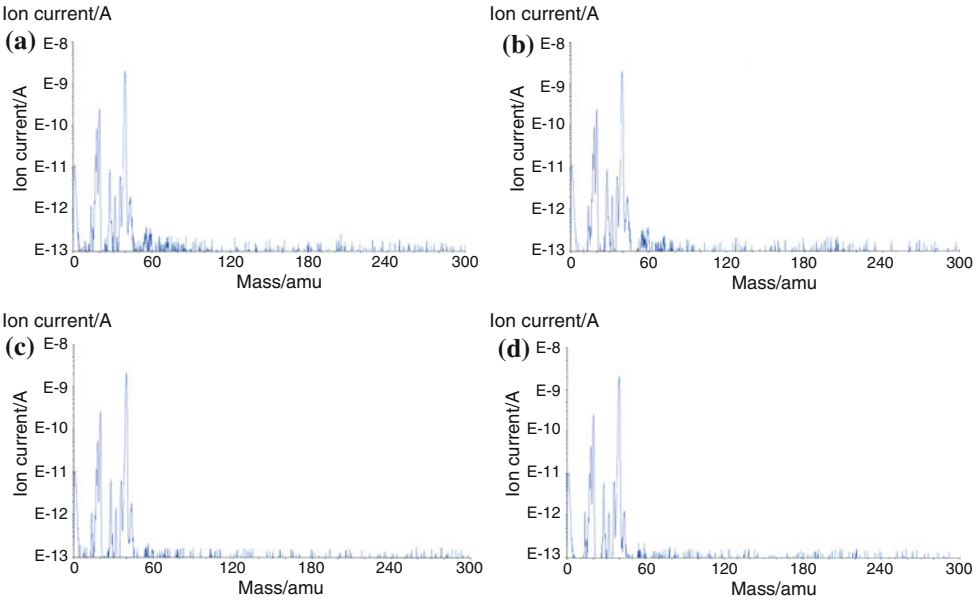

Fig. 9 TG-mass spectroscopy: **a** E30N0 about at 270 °C, **b** E30N2.5 about at 270 °C, **c** E30N0 about at 450 °C, and **d** E30N2.5 about at 450 °C

connecting the chain. When the polymer was being heated, the side groups are stripped off from the chain before it is broken into smaller pieces. The backbone can break down randomly and it could be occurred at any position of the backbone. The molecular mass decreases rapidly, evolving a combination of lower molecular mass fragments along with the monomers. This is because it forms new free radicals which have high activity leading to intermolecular chain transfer and disproportion termination with the $>CH_2$ group. The mechanisms of thermal decomposition have been proposed and summarized in Scheme 2. It has been proposed that initial degradation occurs by side-group elimination (path A), leading to the formation of unsaturated products. At the same time, the scission of main chain (path B) starts. The random scission of EMA is initiated by homolytic scission of a methoxycarbonyl side group followed by β scission. Side-group elimination is a more dominant process than main chain scission at least in the lower temperature ranges.

At high temperatures, the components of the long chain backbone of the polymer can begin to separate (molecular scission) and react with one another. Under thermal effect, the end of polymer chain departs, giving rise to lower yield of free radicals. Then according to the chain reaction mechanism, the polymer loses the monomer one by one. However, the molecular chain does not change a lot within short span of time. The predominant process in the formation of volatiles appears to be intramolecular transfer of radicals.

The average mass fraction of composites (with respect to the total mass) decreased from 90 to 80% as the

Scheme 2 The proposed degradation mechanism of EMA and EMA/MWNTs composites

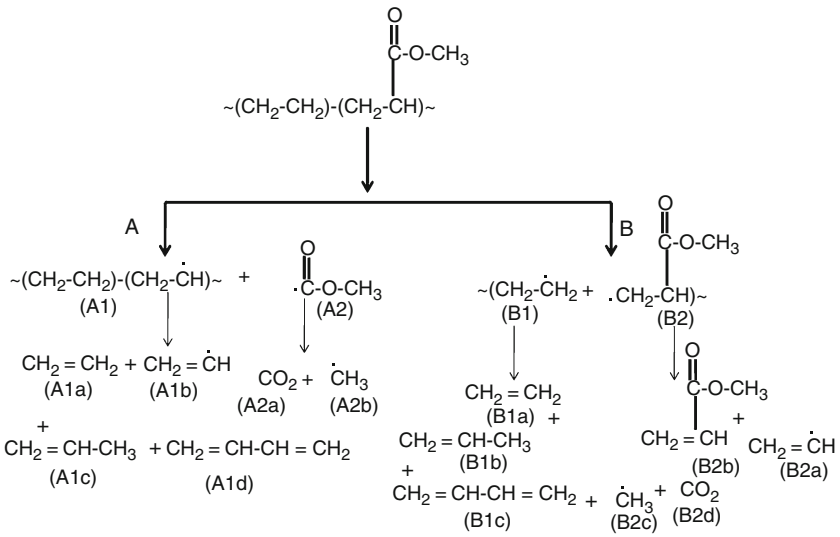

temperature was increased from 300 to 450 °C. Evolution of large number of volatile gaseous species released between 350 and 450 °C confirms the complexity of thermal degradation process. The generation of monomer was accompanied by the formation of a number of low-molecular mass stable species (H_2, CO, CO_2, CH_4, C_2H_4, C_2H_6, and $HCOOCH_3$) in trace amounts.

Scheme 2 lists the structures of the possible degradation products formed from the EMA. The degradation of neat EMA and its composites yield CO_2 (*m*/*z* 44), CH_4 (*m*/*z* 16), CH_2=CH_2 (*m*/*z* 28), $HCOOCH_3$ (*m*/*z* 60), and other MA monomer (*m*/*z* 86). Figures 7, 8, and 9 show intense peaks at *m*/*z* 18 is possibly due to the Ar gas used in TG-mass spectroscopy. Peak corresponding $m/z = 28$ is due to the formation of CH_2=CH_2 from the thermal decomposition of EMA main chain. Figures 7, 8, and 9 also show two intense peaks at high temperature corresponding to $m/z = 40$ and $m/z = 54$ are due to the formation of CH_2=CH–CH_3 and CH_2=CH–CH=CH_2, respectively. This may be due to the thermal decomposition of poly ethylene backbone or EMA main chain. The peak corresponding to *m*/*z* 60 refers to the possible formation of $HCOOCH_3$ from a macro-radical formed after the rupture of a C–$COOCH_3$ bond at the end unit containing an unsaturated bond: The rupture energy of a C–$COOCH_3$ is approximately 10 kcal mol^{-1} less than that of a C–C bond in the main chain [25]. Formation CO_2, CH_4 are due to degradation of –$COOCH_3$ side chain. CO is produced mainly from incomplete combustion of macro-molecular chain. The TG-mass spectrum of neat EMA shows a peak at *m*/*z* 86 probably due to the molecular ion of the MA monomer derived from a macro-radical formed after the scission of backbone.

The *m*/*z* values corresponding to the degradations at 400 and 500 °C were also calculated. The amount of MA produced is clearly dependent on the temperature or degradation time. At 420 °C, more intense peak corresponding to MA was observed than that obtained at 500 °C or above. This shows that there is decreasing involvement of side-group elimination with increasing temperature. It should be noted that even at moderate conversions, the actual degree of decomposition is likely to be different from the initial degradation. For the first 20% conversion, similar amounts of conjugation are produced at all cycle. However, above 20% conversion, unsaturated gaseous fragments are predominating. Accordingly, at high temperatures, the peak corresponding to the ion at *m*/*z* 86 and 60 has not been observed. Most importantly, in terms of stabilization, MWNTs do not offer any preference either to the degradation of side groups or main chain of EMA. However, a gross stabilization effect is observed in general.

Isothermal decomposition

Figure 10a–d shows the isothermal TG curves at fixed temperatures of 375, 400, 425, and 450 °C for EMA09, EMA24, and EMA30-based composites. Composites exhibits a slow and steady decomposition at 375 °C, and the decomposition becomes relatively more rapid with increasing temperature. The single-step mass loss and drastic degradation of EMA have been observed during the first 20 min of isothermal decomposition. The decomposition of EMA30 and its composites becomes relatively more rapid under isothermal heating at higher temperatures viz. 400–450 °C. This relates well with the non-isothermal decomposition in nitrogen as depicted earlier. At higher temperature (450 °C and above), all composites rapidly degrade similar to the respective neat EMAs. This indicates that the thermal stability of the composites contributed from the incorporation of MWNTs is not pronounced at

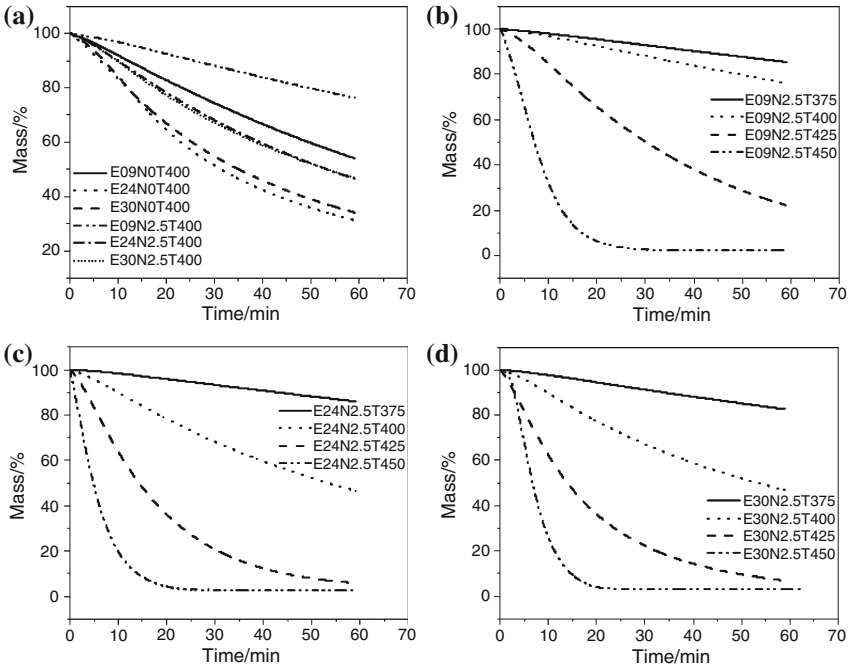

Fig. 10 a–d Isothermal TG curves of pure EMAs and its composites at different temperatures for 60 min in nitrogen atmosphere

higher temperatures. The thermal stabilities of the E09N2.5 nanocomposites are much higher compared to those of the pure EMA containing 9% MA. Distributed MWNTs in E09N2.5 possibly prevent small gaseous molecules permeating out from the nanocomposites during initial stages thermal decomposition and consequently, the composites exhibit higher thermal stability.

The isothermal decomposition data of the neat polymer and their composites, viz., the time at maximum mass loss (t_{max}), and rate of mass loss $(d\alpha/dt)_{max}$ are calculated. The t_{max} of the composites are slightly higher than neat EMA counterparts, whereas, $(d\alpha/dt)_{max}$ values are much higher especially in EMA30-based composites indicating the rapid mass loss. The amount of residue for the neat EMAs and their composites are decreased progressively with raising isothermal set temperatures. Mass loss and mass loss rates have been strongly affected by isothermal set temperature. In addition, it can be noted that rapid degree of mass loss occurs with increase in MA content of the matrix. The masses of the composites remain after 60 min is higher for E09N2.5. High residual mass of the composites indicates that the EMA matrix has not completely degraded at this stipulated time.

Based on the isothermal degradation results (time vs. conversion), fitments have been done considering various order of reactions (0, 0.5, 1.0, 1.5, 2.0, 2.5, and 3.0) with their rate equations. Plot of time versus conversion at a particular temperature for various composites has been carried out. A very good correlation coefficient (R^2 value > 0.98) is observed, indicating a good fit of data (plots are not shown). The decomposition of EMA and its composites follows pseudo-order reaction. As the set temperatures are increased, the minor change in 'n' is observed. The initial reaction order of the samples ranged from 0 to 5 min (first 5 min) does not show good fitment with respect to particular reaction order. The data corresponding to decomposition of initial 5–10 min can be closely fitted with the 1.0 and 1.5 orders. The final parts of data (from 10 to 60 min) fit well with second-order decomposition kinetics. Results show that the overall order of thermal decomposition reaction has been of pseudo first and second, for initial and final phase of decomposition, respectively.

Conclusions

The isothermal and non-isothermal degradation of three EMAs with comparable MFI values in inert atmosphere has been investigated. The analysis of the kinetic parameters of the non-isothermal degradation of the samples confirms that the filled samples are thermally more stable than the unfilled ones. The corresponding kinetic parameters have been evaluated. Composites with EMA09 have higher E_a, hence better thermal stability. The Kissinger model can be applied on TG data for both for pure EMA and EMA/MWNTs systems. The trends of E_a of the various samples are in line with their corresponding order of thermal stability. The results obtained by Flynn–Wall–Ozawa method show that within the conversion degree ranging from 5 to 20%, the fitted straight lines of EMA and EMA/MWNTs composites are nearly parallel, proving the applicability of Flynn–Wall–Ozawa method. TG-mass spectrometric

method has been successfully utilized to predict the reaction mechanism of thermal degradation of pure EMAs and EMA/MWNTs composites based on their decomposition products. Mechanism of thermal degradation has been speculated to be initiated by arrays of side chain and chain scission processes, following pseudo first- and second-order reaction. Mass-spectrometric results quite accurately unveil the picture of thermal degradation of EMA/MWNT systems. The major volatile gases evolved upon thermal decomposition were water, carbon dioxide, methane, carbon monoxide, and MA, respectively.

Acknowledgements The authors are grateful to the Department of Atomic Energy (DAE), Mumbai for funding this project (2007/35/8/BRNS with RTAC, BRNS). One of the authors is highly grateful to CSIR, New Delhi for funding his fellowship to carry out this study.

References

1. Procópio JVV, de Souza VG, da Costa RA, Correia LP, de Souza FS, Macêdo RO. Application of thermal analysis and pyrolysis coupled to GC/MS in the qualification of simvastatin pharmaceutical raw material, J Therm Anal Calorim. 2011. doi: 10.1007/s10973-010-1274-y.
2. Dakka SM. TG/DTA/MS of poly(methyl methacrylate): the role of the oxidative environment. J Therm Anal Calorim. 2003;73:17–24.
3. Wang XL, Yang KK, Wang YZ, Wu B, Liu Y, Yang B. Thermogravimetric analysis of the decomposition of poly(1,4-dioxan-2-one)/starch blends. Polym Degrad Stab. 2003;81:415–21.
4. Iijiama S. Helical microtubules of graphitic carbon. Nature. 1991;354:56–8.
5. Schadler LS, Giannaris SC, Ajayan PM. Load transfer in carbon nanotube epoxy composites. Appl Phys Lett. 1998;73:3842–4.
6. Lourie O, Cox DM, Wagner HD. Buckling and collapse of embedded carbon nanotubes. Phys Rev Lett. 1998;81:1638–41.
7. Ajayan PM, Schadler LS, Giannaris C, Rubio A. Single-walled carbon nanotube-polymer composites: strength and weakness. Adv Mater. 2000;12:750–3.
8. Cooney JD, Day M, Wiles DM. Thermal degradation of poly(ethylene terephthalate): a kinetic analysis of thermogravimetric data. J Appl Polym Sci. 1983;28:2887–902.
9. Liu W, Li G. Non-isothermal kinetic analysis of the thermal denaturation of type I collagen in solution using isoconversional and multivariate non-linear regression methods. Polym Degrad Stab. 2010;95:2233–40.
10. Lee JY, Shim MJ, Kim SW. Thermal decomposition kinetics of an epoxy resin with rubber-modified curing agent. J Appl Polym Sci. 2001;81:479–85.
11. Kissinger HE. Reaction kinetics in differential thermal analysis. Anal Chem. 1957;29:1702–6.
12. Sivalingham G, De P, Karthik R, Madras G. Thermal degradation kinetics of vinyl polyperoxide copolymers. Polym Degrad Stab. 2004;84:173–9.
13. Mongal N, Chakraborty D, Bhattacharyya R, Chaki TK, Bhattacharya P. Effect of electron-beam irradiation on ethylene–methyl acrylate copolymer. J Appl Polym Sci. 2009;112:28–35.
14. Basuli U, Chaki TK, Chattopadhyay S, Sabharwal S. Thermal and mechanical properties of polymer-nanocomposites based on ethylene methyl acrylate and multiwalled carbon nanotube. Polym Compos. 2010;31:1168–78.
15. Basuli U, Chaki TK, Sabharwal S, Chattopahdyay S. Influence of acrylate content on the properties of ethylene methyl acrylate-multi walled carbon nanotube composites. Adv Sci Lett. 2010;3:10–9.
16. Borah JS, Chaki TK. Thermogravimetric and dynamic mechanical analysis of LLDPE/EMA blends. J Therm Anal Calorim. 2011. doi: 10.1007/s10973-011-1489-6.
17. Chou YC, Hsieh TF, Hsieh YC, Lin CP, Shu CM. Comparisons of MWCNTs and acidified process by HNO_3 on thermal stability by DSC and TG-FTIR. J Therm Anal Calorim. 2010;102:641–6.
18. Vyazovkin S. Kinetic concepts of thermally stimulated re-actions in solids: a view from a historical perspective. Int Rev Phys Chem. 2000;19:45–60.
19. Wang H, Yang J, Long S, Wang X, Yang Z, Li G. Studies on the thermal degradation of poly (phenylene sulfide sulfone). Polym Degrad Stab. 2003;83:229–35.
20. Zhong R, Hu Y, Wang S, Song L. Thermogravimetric evaluation of PC/ABS/montmorillonite nanocomposite. Polym Degrad Stab. 2004;83:423–8.
21. Ozawa T. A new method of analyzing thermogravimetric data. Bull Chem Soc Jpn. 1965;38:1881–6.
22. Flynn JH, Wall LA. A quick, direct method for the determination of activation energy from thermogravimetric data. Polym Lett. 1966;4:323–8.
23. Doyle CD. Estimating isothermal life from thermogravimetric data. J Appl Polym Sci. 1962;6:639–42.
24. Rosu D, Cascaval CN, Ciobanu C, Rosu L. An investigation of the thermal degradation of epoxy maleate of bisphenol A. J Anal Appl Pyrolysis. 2004;72:191–6.
25. Shibaev LA, Antonova TA, Vinogradova LV, Ginzburg BM, Ginzburg VG, Zgonnik VN, Melenevskaya EYu. Mass-spectrometric investigation of the thermal stability of polymethyl methacrylate in the presence of C_{60} fullerene. Tech Phys Lett. 1997;23:730–1.